diffusion-fundamentals

The Open-Access Journal for the Basic Principles of Diffusion Theory, Experiment and Application

Diffusion in Nanocrystalline Solids

Alan V. Chadwick

Functional Materials Group, School of Physical Sciences, University of Kent, Canterbury, Kent CT2 7NR, UK

E-Mail: a.v.chadwick@kent.ac.uk

Abstract

Enhanced atomic migration was an early observation from experimental studies into nanocrystalline solids. This contribution presents an overview of the available diffusion data for simple metals and ionic materials in nanocrystalline form. It will be shown that enhanced diffusion can be interpreted in terms of atomic transport along the interfaces, which are comparable to grain boundaries in coarse-grained analogues. However, the method of sample preparation is seen to play a major role in the experiments and there are still many gaps in understanding the detailed mechanisms of diffusion in these systems.

Keywords:- Nanocrystals, diffusion, metals, ionic conductivity, grain boundaries, interfaces.

1. Introduction

Nanomaterials are systems that contain particles with one dimension in the nanometre regime. Currently there is intense interest from biologists, chemists, physicists and engineers in the application of these materials, so-called *nanotechnology*, which is sometimes referred to as '*the next industrial revolution*' [1]. The reason for the interest is the unusual properties, very often with useful applications, that are exhibited by these materials when compared to their bulk counterparts [2-10]. In this article we will focus on rather simple inorganic solids, mainly metals and ionic solids, with dimensions predominantly less than 100 nm. In these systems the origin of the unusual properties is twofold; (i) the fact that the dimension of the particles approaches, or becomes

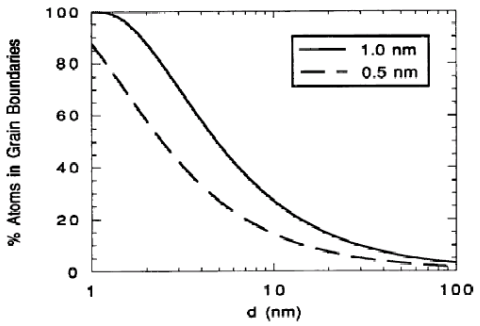

Fig 1. Percentage of atoms in grain boundaries as a function of grain size assuming boundary widths of 0.5 and 1 nm. (after [15])

smaller than, the critical length for certain phenomena (e.g. the de Broglie wavelength for the electron, the mean free path of excitons, the distance required to form a Frank-Reed dislocation loop, thickness of the space-charge layer, etc.) and (ii) surface effects dominate the thermodynamics and energetics of the particles (e.g. crystal structure, surface morphology, reactivity, etc.). In nanostructured semiconductors it is the first of these, which leads to special electrical, magnetic and optical properties and the possibility of *quantum dot* devices. The second factor can lead to nanocrystals adopting different morphologies to bulk crystals with different exposed lattice planes leading to an extraordinary surface chemistry [11-12] and catalytic activity [13,14]. The importance of surfaces and boundaries in nanocrystalline systems is demonstrated in Fig.1, which shows the fraction of atoms in these regions as a function of grain size.

As one example of the special properties of nanocrystalline metals and ionic crystals it is worth considering the simple mechanical properties as these are clearly controlled by diffusion, the topic of this article. A great deal of research has focused on the mechanical properties of compacted nanocrystalline materials, as their behaviour is extremely unusual [16]. Firstly they can exhibit '*superhardness'* as the individual grains are smaller than the distance required to form a Frank-Reed loop, thus the isolated grains are expected to be very hard. Normal polycrystalline samples of metals follow the Hall-Petch equation, which can be expressed in the form [16]:-

$$H_v = H_o + k_h d^{-1/2} \qquad (1)$$

where H_v is the indentation hardness and H_o and k_h are constants. In samples with normal grain sizes this is interpreted as the grain boundaries acting as obstacles to the motion of dislocations. As the grain size moves into the nanometre regime the slope of the Hall-Petch plot (H_v *versus* $d^{-1/2}$) decreases. At about 20 nm the plot either plateaus or reverses slope (referred to as *inverse Hall-Petch* behaviour). This is demonstrated in Fig. 2 where collected data for Cu are shown [17]. There is some debate concerning the validity of the inverse Hall-Petch behaviour and it may be a feature of the sample preparation, i.e. gas pores, impurities in the boundaries, etc. The apparent softening at very small sizes is seen in samples prepared by inert gas condensation and compaction but not in films made by electrochemical deposition. Another general feature of nanocrystalline solids is that they exhibit *'superplasticity'*, the ability to undergo very large extensions under tensile stress at low temperatures. For example, it has been reported that electrodeposited nanocrystalline copper exhibits an

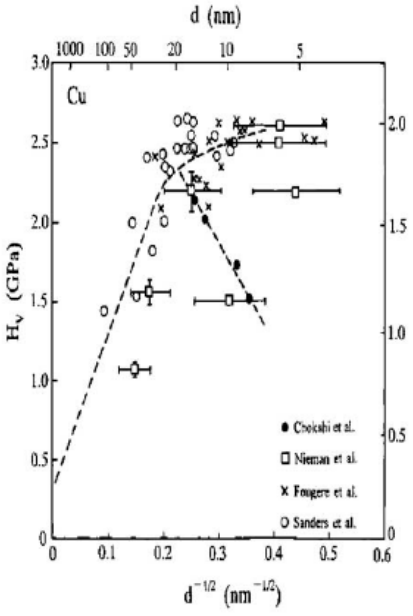

Fig. 2. A Hall-Petch plot for nanocrystalline Cu (after [17]).

elongation higher than 5000% upon rolling at room temperature [18]. The processes giving rise to this effect are a combination of grain boundary sliding, grain rotation and atomic diffusion. A phenomenological equation which describes this behaviour can written as:-

$$\dot{\varepsilon} = A \frac{DGb}{kT} \left(\frac{b}{d} \right)^p \left(\frac{\sigma}{G} \right)^n \qquad (2)$$

where ε is the strain rate, D is the average diffusion coefficient, G is the shear modulus, b is the Burgers vector, k is the Boltzmann constant, d is the grain size, T is absolute temperature, p is the grain size exponent, s is the applied stress and n is the stress exponent. The grain size exponent (p) has a value between 2 and 3, depending upon whether lattice diffusion or grain-boundary diffusion is the controlling mode of deformation. Clearly, if we are to gain an understanding of the unusual mechanical properties we need information on the basic diffusion processes in nanocrystalline solids.

There are many other properties of nanocrystalline materials where diffusion plays a dominant role. Recent reviews cover diffusion in nanocrystalline metals [9,19] and ceramics [20]. In addition, a comprehensive review of the mechanical properties of nanocrystalline materials is available [16]. However, definitive transport experiments are difficult to perform and for several systems there is debate about the reliability of the experimental data and a consistent picture of the diffusion mechanisms is still emerging. The aim here is to present a critical overview of the current state of knowledge of atomic diffusion in nanocrystalline metals and ionic solids. In order to achieve this aim the article has been divided into various sections. The first section will briefly describe the experimental methodology used in the study of nanocrystalline solids. In addition to the diffusion methods this section will also include sub-sections on the preparation of samples, the characterisation of size and microstructure. This is particularly important as it is now quite clear that the microstructure, and hence the properties, of nanocrystalline materials are very dependent on the preparation technique. The second section will review the experimental data, considering those available for metals and ionic solids in separate sub-sections. The final section will simply draw together the information into conclusions on the mechanisms of diffusion in nanocrystalline solids.

2. Experimental Methodology

2.a Preparation of nanocrystalline samples

A very wide variety of methods have been employed to produce nanocrystalline samples and only the more commonly used ones will be considered. Inert gas condensation (IGC) has been extensively used to fabricate metallic and metal-oxide powders with a well-defined and narrow size distribution [2,21]. The apparatus is shown in Fig. 3. The metal is evaporated inside an ultrahigh vacuum (UHV) chamber filled with a low pressure of inert gas, typically helium. Vapours from the hot source migrate into a

cooler gas by a combination of convective flows and diffusion. The vaporized species then lose energy via collisions with inert gas molecules. As collisions limit the mean free path, supersaturation can be achieved above the vapour source, the vapours rapidly nucleate, forming large numbers of clusters that grow via coalescence and agglomeration. The clusters entrained in the condensing gas are transported by convection to a liquid nitrogen filled cold finger. The particles are removed from the cold finger by means of a scraper assembly, are collected via a funnel and transported to an in-situ compaction device. The amount of material that can be produced is relatively small and there have been several modifications to increase the yield using sputtering methods [22-25].

Spray pyrolysis is a fairly general method of producing nanocrystalline oxides. In this case a solution of a chemical precursor is dispersed into the gas phase as aerosol droplets. The droplets are then transported to a hot zone where they are decomposed to form oxide particles. This method has relatively wide applicability and has been used to prepare several metal oxide nanoparticles such as ZnO, ZrO_2 and Al_2O_3 [26].

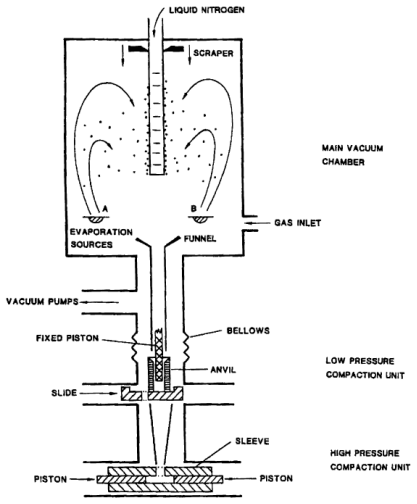

Fig. 3. Inert-gas condensation facility for the synthesis of nanocrystalline particles (after [21]).

Sol-gel procedures have been used for many years to produce oxides and ceramics offer control over the structure and composition at the molecular level [27,28]. The usual procedure is to subject metal alkoxides $M(OR)_x$ to controlled hydrolysis, replacement of the OR group by OH. This leads to the formation of a sol, very small colloidal particles, which then condense to form a gel, an inter-connected network. The gel is then dried and the final product can be either oxide (as in the case of silicon tetraethyl orthosilicate) or hydroxide (zirconium iso-propoxide) or a mixed methoxy-hydroxide (as in the case of magnesium methoxide). Thus the final step in the formation of the oxide is calcination at high temperature. This step is difficult to control and presents two major problems, as exemplified by recent work on ZrO_2 [29]. If the calcining temperature is too low then all of the residual OH may not be completely removed from the material. If the calcination temperature is too high then the

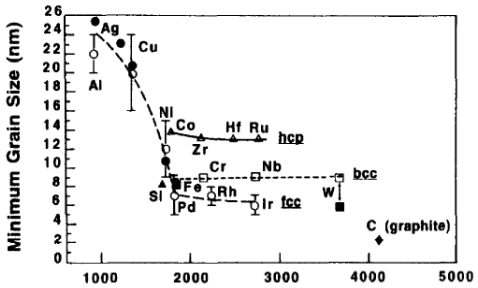

Figure 4. Variation of minimum grain size with melting temperature (abszissa, in K; after [32]).

particles will grow and the nanocrystallites will be lost. The surface energy of nanocrystals is such that relatively moderate temperatures (~400°C in the case of most oxides) will lead to measurable grain growth over the period of a few minutes [30].

An apparently completely general method of producing all forms of nanocrystals is by mechanical attrition. This involves taking bulk material and reducing the grain size in a high-energy ball mill. [31-34]. The final minimum grain size that can be achieved depends on the melting point of the material, as shown in Fig. 4. The advantages of ball milling are the fact that almost every material is accessible, that large amounts can be produced and that the average grain size can easily be varied by choice of the milling time. In addition, it is possible to produce materials *in situ* in the ball mill by double decomposition reactions [35,36]. This method is therefore useful when many different materials are to be compared. One disadvantage of ball milling is that abrasion of the milling media may occur. This has to be minimized by choosing appropriate materials for the milling vial and balls, respectively. A further disadvantage is that the milling can produce amorphous debris, to the extent that recent work on ball milled Al_2O_3 indicated that the sample consisted of nanocrystalline grains embedded in amorphous material [37].

2.b Determination of particle size

The determination of the particle size of a material is usually the first step in any investigation of a nanocrystalline sample. Generally there are three approaches that can be employed; X-ray powder diffraction, electron microscopy and the measurement of the surface by BET gas adsorption. A critique of the three methods, exploring the advantages and disadvantages, has recently been published as a result of a study of TiO_2 [38].

X-ray powder diffraction is a technique that can be employed for almost all samples. Peak broadening as the particle size decreases is a well-known phenomenon [39] and can be used to determine the particle size, *s*, *via* the Scherrer equation, namely:-

$$s = \frac{k\lambda}{\beta \cos\theta} \qquad (3)$$

where k is a constant (usually taken as 0.9), λ is the wavelength of the X-ray beam, β is the full width at half maximum height (FWHM) of a given peak (after removal of the instrumental broadening) and θ is the diffracted angle of the peak. Eq. 3 represent the simplest treatment of peak broadening and it can be extended to include the effect of strain broadening of the peaks [40]. Clearly, this method will only yield an average particle size and will not provide information on the dispersion of the size or the extent of agglomeration of the grains. However, it is possible to gain some insight into the particle shape by taking data from different diffraction peaks.

Gas adsorption measurements are usually performed with nitrogen or an inert gas with the sample at –196°C. The surface area, *S,* is determined using the classical BET approach [41]. The particle size, s_{BET}, from these measurements is given by [42]:-

$$s_{BET} = \frac{6}{\rho S} \qquad (4)$$

where ρ is the density. The factor of 6 applies for spherical and cubic particles.

Transmission electron microscopy (TEM) is essentially the ideal method of determining particle size, however sample preparation can present difficulties. Provided a sufficiently large number of grains in the sample are observed the size dispersion and degree of agglomeration can be measured. In addition, electron micrographs will reveal information on the microstructure of the sample.

The three techniques have their advantages, disadvantages and pitfalls, however the overall agreement between them is relatively good [38].

2.c Determination of the microstructure

The microstructure is the key to the properties of nanocrystalline materials. It was seen earlier that simple geometric considerations lead to the conclusion that a large fraction of the atoms in a nanocrystal are in the surface (see Fig. 1). However, crucial questions are the nature of the surface, in terms of the level of atomic order, and the structure of the interface between grains. Two extreme possibilities are shown in Fig. 5. One extreme, shown schematically in Fig. 5a, is that there is extensive disorder in an interface that is several atoms in width. In this figure the black circles represent atoms in the grains and the open circles are the atoms in the interfaces. In some of the early work on nanocrystals this was intuitively assumed to be the case and the interfaces were referred to as 'gas-like' or 'liquid-like'. This structure would clearly account for rapid diffusion in nanocrystalline samples. The alternative view, shown in Fig. 5b, is that the interface is similar to a grain boundary in normal bulk materials. In this case the interfaces would exhibit usual behaviour, although they would be present in unusually large number.

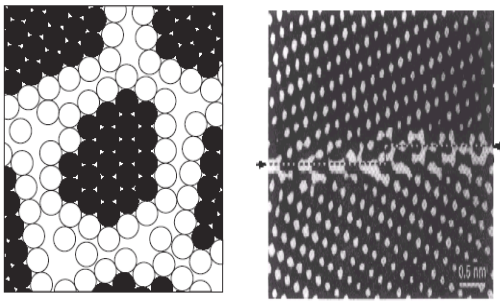

(a) (b)

Fig.5. Two possible models for the interface between nanocrystalline grains; (a) disordered interface, (b) a 'normal' grain boundary'.

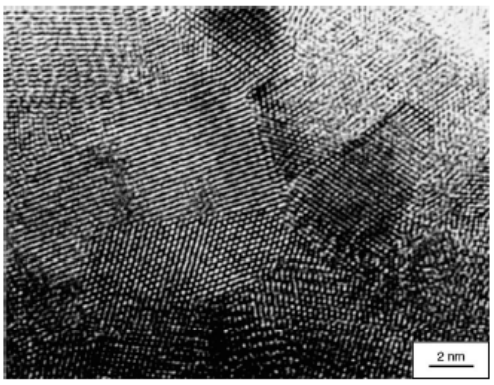

Fig. 6. HRTEM image of a region of nanocrystalline palladium containing a number of grains (after [43]).

High resolution TEM can provide the microstructural details and an example is shown in Fig. 6, a micrograph of nanocrystalline palladium. The

HRTEM image of the interfacial grain boundaries shows flat facets interspersed with steps [43]. There is no evidence for highly disordered interfaces and this appeared consistent with other studies [43]. Similarly, TEM measurements on nanocrystalline ceria showed that the grains had a high degree of perfection and were separated by sharp, boundaries [44]. Unfortunately the data from HRTEM studies are relatively sparse and other structural techniques have had to be used to explore the microstructure, such as electron diffraction [45], positron annihilation spectroscopy [46] and extended X-ray absorption fine structure (EXAFS) measurements [47-49].

EXAFS are the oscillations in the X-ray absorption (a plot of absorption coefficient, μ, *versus* incident photon energy) that occur beyond the absorption edge for the emission of a core (K or L shell) electron [50-52]. The oscillations arise from the emitted photoelectron wave being backscattered and interfering with the outgoing wave. If the two waves are in phase there will be constructive interference, a lower final state energy and a higher probability for absorption. If the two waves are out of phase then there will be destructive interference, higher final state energy and a lower probability for absorption. Thus as the incident photon energy increases so does the energy of the emitted photoelectron with consequential changes on its wavelength. Since the distance between the target atom and its neighbours is fixed there will be shifts in and out of phase and hence the observation of the EXAFS oscillations. The intensity of the oscillations depends on the number and type of neighbours giving rise to the backscattering and an EXAFS Debye-Waller factor (an uncertainty in the distance between target and scattering atoms). EXAFS does not rely on long-range order and is sensitive to the local environment of the target atom out to 5 Å. The Fourier transform of the EXAFS yields a partial radial distribution function in real space with peak areas proportional to average coordination numbers and the Debye-Waller factors.

For a nanocrystalline sample the EXAFS signal could be attenuated for two reasons; (i) the particle is so small that the average coordination numbers for the neighbouring shells is reduced or (ii) there is sufficient disorder in the sample (e.g. at the interfaces) that the Debye-Waller factors are increased. At first sight it would appear that EXAFS has little to offer as a microstructural probe, however for (i) to be operative the particle size has to be very small, typically less than 5 nm. Thus in principle EXAFS can probe disorder in the interfaces of nanocrystals. However, the results have been very confusing and the subject of much argument. The EXAFS data for ZrO_2 represent a typical example. There have been several EXAFS studies of this system, which claim evidence for disordered interfaces in nanocrystalline samples, i.e. an attenuation of

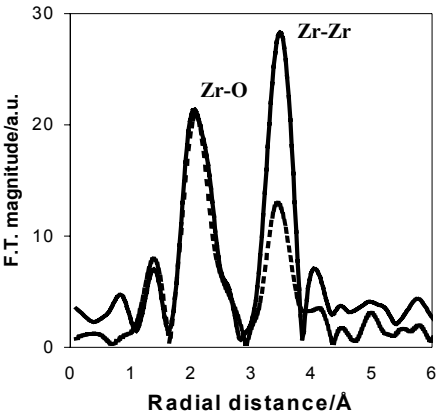

Fig. 7. Fourier transform of the EXAFS spectra for ZrO_2. Solid line is bulk material. Dashed line is for ball-milled material with a grain size of 15 nm (after [56]).

the EXAFS for the Zr-Zr correlation [53,54]. However, similar measurements on carefully prepared films, with particle sizes down to 6 nm found the EXAFS was indistinguishable from the bulk [29,49,55] and great care has to be taken to ensure all hydroxyl species are removed from the sample. In contrast, the EXAFS of ball-milled ZrO_2, with a grain size of 15 nm (too large to show any reduction of the average coordination number) shows a marked reduction of the Zr-Zr correlation [56], as shown in Fig. 7. This was interpreted as the presence of amorphous material in the ball-milled sample, analogous to the study of ball-milled Al_2O_3 [37]. Similar effects were observed in the EXAFS of other ball-milled oxides, for example $LiNbO_3$ [57]. In general, the EXAFS of sol-gel prepared nanocrystalline oxides (ZrO_2, SnO_2, CeO_2, ZnO) show no evidence of excessive disorder [49].

EXAFS studies of nanocrystalline metals have also been controversial [58]. However, again sample preparation has been shown to be important. The EXAFS studies of 13 nm grain size Cu, for a sample that had not been machined, showed a spectrum that was not attenuated and close to that for bulk Cu [58]. This provided evidence for interfaces that were similar to normal grain boundaries.

2.d Measurement of atomic transport

A very wide range of techniques can be used to probe atomic transport. An elegant survey of the methods can be found in the work of Heitjans [20,59,60]. A useful division is into macroscopic techniques, which measure the effect of long-range motion of atoms, and microscopic techniques, which measure jump frequencies of atoms. In principle the two are inter-connected by the Einstein-Smoluchowski equation:-

$$D = \frac{1}{6}\frac{a^2}{\tau_c} \qquad (5)$$

where D is the diffusion coefficient, a is the length of a jump and τ_c is the motional correlation time (the time between diffusive jumps). The ranges of D and τ_c accessible to the various techniques are summarised schematically in Fig. 8. The diffusion coefficient is expected to show Arrhenius behaviour:-

$$D = D_o \exp\left(\frac{-Q}{kT}\right) \qquad (6)$$

where D_o is the pre-exponential factor, Q is the activation energy and k is the Boltzmann constant.

Tracer diffusion is the classical macroscopic technique [60]. In these experiments an isotopic tracer of the atom under study is diffused into the sample for a known time at a fixed temperature. Sections are then removed from the sample, the sections analysed for the tracer concentration, the penetration profile determined and D determined from the boundary conditions [61]. For penetration depths larger than 1 μm classical radiotracer techniques can be used, which implies mechanical sectioning of the

specimen and subsequent measurement of radioactivity of the sections. By contrast, SIMS (secondary ion mass spectrometry) profiling is applicable for penetration depths smaller than 1 μm. The surface of the specimen is bombarded with a beam of primary ions, which results in a continuous atomisation of the sample. The sputtered secondary ions can then be detected in a mass spectrometer. An advantage of the tracer technique is that since the profile is determined it is often possible to separate out different diffusion process (e.g. bulk, grain boundary, surface diffusion, etc.) provided they have sufficiently different diffusivities.

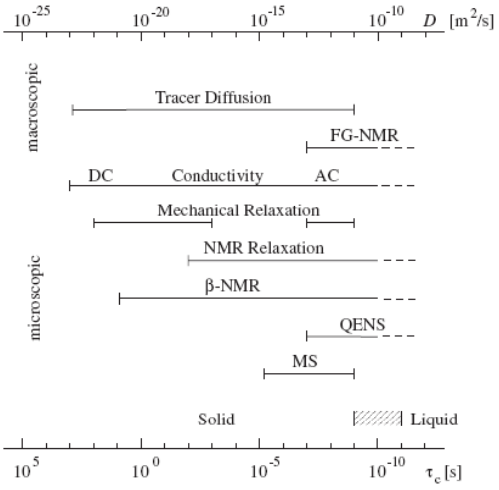

Fig. 8. Typical ranges of the diffusivity D and motional correlation time τ_c of some macroscopic and microscopic methods, respectively, for studying diffusion in solids. FG-NMR: field gradient NMR, β-NMR: β-radiation-detected NMR, QENS: quasi-elastic neutron scattering, MS: Mössbauer spectroscopy. The hatched bar indicates the transition from the solid to the liquid where the motional correlation time is reduced by about two orders of magnitude (from [20]).

Nuclear magnetic resonance (NMR) spectroscopy offers a range of methods for studying diffusion in the solid state [62,63]. If the diffusion is sufficiently fast in the solid (D>10^{-13} m^{2}s^{-1}) then field gradient NMR methods can be employed. In this case, the nuclear spin is essentially used as a label (like a tracer), to follow the motion of the atoms over many jump distances. The diffusion coefficient can be determined directly from the measurement without the need to resort to a theoretical model. Thus this is a macroscopic method.

A very wide range of diffusivity is accessible to NMR relaxation measurements. The diffusive motions of the nuclei can affect the relaxation times of the nuclear spins, following a perturbance of the spin system by the application of a magnetic field. In simple terms, the moving spins will create oscillating magnetic fields that will interact with the spin system. Thus the NMR relaxation times T_1 (spin-lattice relaxation time), T_2 (spin-spin relaxation time), $T_{1\rho}$ (spin-lattice relaxation time in the rotating frame), etc., can all provide information on diffusion. However, the time scale of the measurement is very short, such that the atoms traverse very few atomic distances and NMR relaxation time is a microscopic method. Except in special cases it is very difficult to obtain accurate values of D from the measured relaxation times due to complexities in the theoretical models [63]. However, relative values are precise and accurate values of Q can be evaluated.

NMR lineshape spectroscopy [20] is another NMR diffusion technique. The linewidth of the resonance line is inversely proportional to T_2 and hence is affected by diffusion. In a solid the resonance line is very broad, however as the nuclei begin to diffuse with increasing temperature the line narrows, referred to as *motional line narrowing*. Thus the line width is inversely proportional to D and the measurements provide a simple and direct means of studying diffusion.

Before leaving the NMR techniques it is worth noting that for a number of particularly important elements they provide a convenient (in some cases the *only*) method of studying atomic diffusion. These include ^{7}Li, ^{17}O and ^{19}F, elements where the radiotracers are non-existent or very short-lived.

For ionic solids the measurement of the ionic conductivity, σ, has long provided a method of studying the atomic diffusion [64-66]. The early studies were restricted to measurements on single crystals and in this case σ and the tracer diffusion coefficient, D^T are related by the Nernst-Einstein equation [64]:-

$$D^T = \frac{H_r \sigma\ kT}{Nq^2} \qquad (7)$$

Here H_r is the Haven ratio, N is the particle density and q is the charge of the mobile ion. Eq. 7 assumes that only one of the ions in the crystal is mobile. The Haven ratio is related to the degree of correlation of the ionic jumps. For jumps involving single point defects it is accurately known for the different crystal structures. Ionic conductivity measurements, coupled with other diffusion measurements, have proved a very powerful method of identifying diffusion measurements. However, the requirement of single crystal samples was very restricting in terms of the materials that could be investigated.

Impedance spectroscopy is the measurement of the complex impedance over a wide range of a.c. frequency and is an important tool to study diffusion in solids [20, 66-70]. The advantage of this technique is that it can be used to study polycrystalline and compacted samples and it can deconvolute the contributions from the different structural components of the sample like bulk material or grain

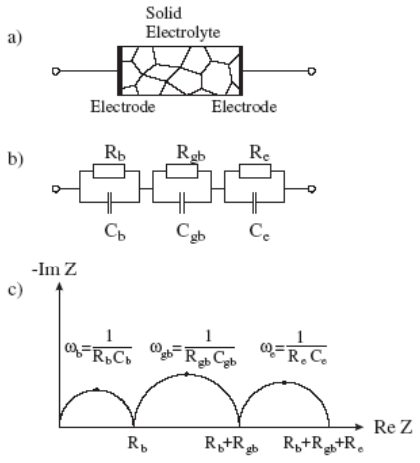

Fig. 9. (a) Polycrystalline solid electrolyte with contacts, (b) equivalent circuit with contributions from (the bulk of) the grains, the grain boundaries and the electrodes and (c) impedance plot for the case $\omega_b >> \omega g_b >> \omega_e$ (from [20]).

boundaries. The principle of the technique relies on the fact that an RC circuit can describe the total impedance of a sample. If the various components, such as the intra-grain impedance, grain boundary impedance and electrode interface impedance are sufficiently different they will be separable in a complex impedance plot. An idealised example is shown in Fig. 9, where the components are connected in series and the component frequencies differ by two orders of magnitude.

3. Review of the Experimental Information

Before we consider the experimental data it is worth considering some of the experimental difficulties. Since the very earliest measurements of atomic diffusion in solids it has been recognised that surfaces, dislocations and grain boundaries have higher diffusivities than in the bulk lattice [71]. In classical serial sectioning tracer experiments evidence for diffusion along these interfaces can often be seen in the diffusion profile; the profile exhibits two regions, a portion at short penetration due to bulk lattice diffusion, D_B, a portion at deeper penetrations where the tracer has diffused along these *'short-circuiting paths'*. In a polycrystalline sample the dominant fast path for diffusion is the grain boundaries. Thus it is possible but generally with some difficulty, to extract a contribution from grain boundary diffusion coefficient, D_{gb}, from the profiles. Typically D_{gb} is orders of magnitudes larger than D_B, as seen in the data from an extremely thorough study of NiO [72]. The difficulties arise in devising experiments that can determine D_{gb}, separating it from D_B. It is often the case that what is determined is the product δD_{gb} the product of the grain boundary diffusion coefficient and δ the width of the grain boundary [71].

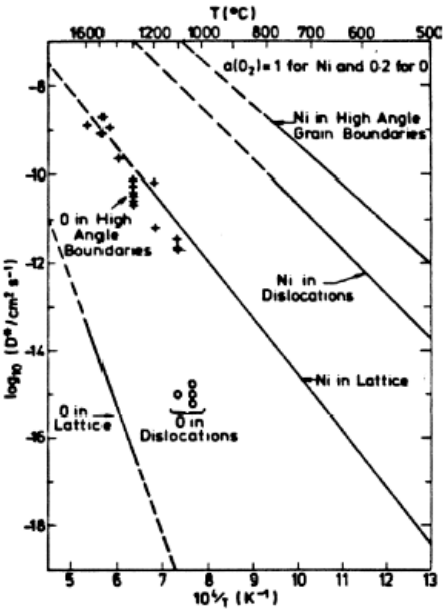

Fig. 10. Nickel and oxygen self-diffusion in bulk, in dislocation and in grain boundaries of nickel oxide (after [72]).

There are other difficulties in attempting to use the classical tracer approach to measure diffusion in nanocrystalline solids. An attempt to show the complexities of the system is shown in Fig. 11. In addition to the lattice and grain boundary diffusion there is also the possibility of diffusion in the interfaces between the potentially wider interfaces between the agglomerates of nanocrystals, shown with a width of δ_A and diffusion coefficient D_A. To some extent this is still a simplification of a real system. For example, there could be gas-filled pores and voids between the grains if the sample has been prepared by compaction. There are two further potential experimental

complications. Firstly, there could be segregation of impurities into the boundaries, which could block or enhance the diffusion of the tracer. Secondly, during the experiment there can be growth and movement of the grain boundaries during the experiment, which would affect the diffusion profile.

The effect on the microstructure of the preparation method used to form the sample has already been outlined in Section 2. This could clearly affect the results of diffusion experiments and must be borne in mind when discussing the data. In addition, it is important to note the specific features of the experimental technique that is used to monitor the atomic transport in nanocrystals, as it will affect the interpretation of the data.

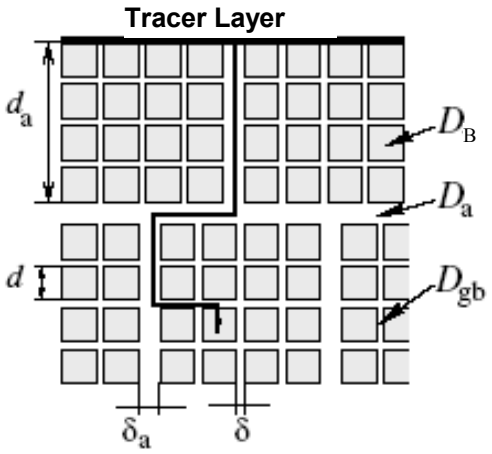

Fig. 11. A schematic model for tracer diffusion in a compacted nanocrystalline sample. D_B is the bulk lattice diffusion coefficient, D_{gb} is the grain boundary diffusion coefficient, D_A is the inter-agglomerate diffusion coefficient, d is the grain size, δ is the width of the grain boundary and δ_A is the separation between agglomerates.

3.a Metals and alloys

A status report on diffusion in nanocrystalline metals and alloys has recently been published [73]. Fast diffusion has long been recognised as a feature of nanocrystalline samples [2-10]. Very early measurements of the self-diffusion in nanocrystalline Cu with a grain size of about 8 nm (produced by means of inert gas condensation and consolidation) [74] showed that the activation energy for diffusion is 0.64 eV, comparable to that for surface diffusion, being only 1/3 of the lattice diffusion. The diffusivities were found to be about 16 orders of magnitude larger than the lattice values. A comparison of the diffusion of hydrogen in a consolidated nanocrystalline Pd (with an average grain size of 5 nm) with that in a Pd single crystal in a large range of H concentration [75], it was found that the diffusion coefficient in the nanocrystalline Pd is several times of the lattice diffusivity at higher H concentrations.

In general, the enhanced diffusion in nanocrystalline metals and alloys can be attributed to diffusion along the grain boundaries, although the nature of sample preparation must always be borne in mind. A case in point is the diffusion of ^{59}Fe in nanocrystalline Fe prepared by compaction of IGC material [76]. The samples were 91-96% theoretical density and the grain size was 19-38 nm. The data are shown in Fig. 12. The self-diffusion coefficients are similar to or slightly higher than the values estimated for the conventional GB diffusion by extrapolating high temperature diffusion data to lower

temperatures. A time-dependent decrease of the apparent self-diffusivities was observed that was probably due to structural relaxation of the interfaces and to interface migration effects.

There is no intrinsic reason for the grain boundaries in nanocrystalline materials to be different from those in bulk samples, and the experimental evidence outlined in Section 2c supports this view. However, as discussed earlier, diffusion along the boundaries between agglomerates could lead to very fast diffusion. In a very elegant study of the Fe, Ni and Ag diffusion in Fe – 40wt%Ni alloy prepared by ball milling with the average grain size of about 30 nm it was possible to separate out the diffusion between the agglomerates [80]. The diffusivities along the grain boundaries and along the inter-agglomerate paths are shown in Fig. 13. The diffusivity of the inter-agglomerate boundaries exceeds that of nanocrystalline grain boundaries by several orders of magnitude and the relevant activation enthalpy (Q_a = 91 kJ/mol) was substantially smaller than the activation enthalpy of nano-GB diffusion (Q_{gb} = 126 kJ/mol). The absolute diffusivities D_a and D_{gb}, , obey the relationship $D_a >> D_{gb}$ in the whole temperature interval of the investigation. The activation enthalpy for inter-agglomerate diffusion was similar to that for surface diffusion.

Finally it is worth noting that a study of diffusion in Cr in a nanocrystalline film of Fe produced by surface mechanical attrition (SMAT) showed that the diffusivity of Cr was 7–9 orders of magnitude higher than that in bulk Fe and 4–5 orders of magnitude higher than that in the grain boundaries of α-Fe [83]. The activation energy for

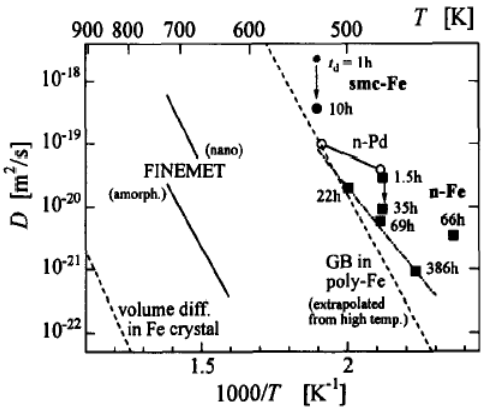

Fig. 12. Arrhenius plot of ^{59}Fe diffusion coefficients for nanocrystalline metals, crystalline (c-) Fe [77], grain boundaries (GBs) in polycrystalline Fe [78] and the Finemet alloys [79] (after [76]).

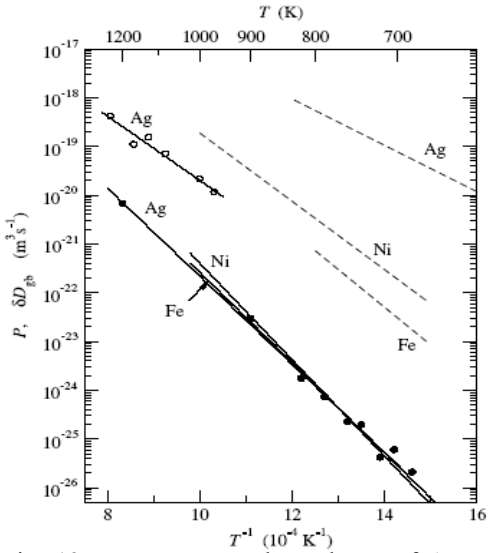

Fig. 13. Temperature dependence of Ag, Fe [81], and Ni [82] diffusion along nanocrystalline GBs in nanocrystalline Fe – 40wt%Ni alloy (solid lines). The diffusivities along inter-agglomerate boundaries are shown by dashed lines (after [80]).

Cr diffusion in the Fe nanophase was comparable to that of the grain boundary diffusion, but the pre-exponential factor is much higher. The enhanced diffusivity of Cr may originate from a large volume fraction of non-equilibrium grain boundaries and a considerable amount of triple junctions in the sample produced by the SMAT technique.

3.b Ionic solids

Diffusion and ionic conduction in nanocrystalline ceramics has recently been reviewed [20]. The interest in these materials dates back to the observation that compacting a 'normal' ionic crystal with fine particles of an insulating oxide, e.g. LiI and Al_2O_3, gives rise to a much-enhanced ionic conductivity [84]. In these systems, referred to as '*dispersed ionic conductors'* the origin of the high conductivity has been assigned to conduction along the interfaces between the ionic and insulating solids. The effect has been quantitatively interpreted in terms of heterogeneous doping and the effect of the *space-charge layer* [85-88]. For a normal, pure MX ionic crystal the concentrations component defects of the defect pair (e.g. cation and anion vacancies in the case of Schottky disorder) in the bulk will be equal due to the constraint of electrical neutrality, even though the formation energies may differ. In the surface of an ionic crystal the constraint is not present and the relative defect concentration, ζ_o, can differ from unity. This effect, referred to in the early literature as the Frenkel-Lehovec space charge layer [64], decays away in moving from the surface to the bulk and can be treated by classical Debye-Hückel theory [85-88]. This leads to a Debye screening length, L_D, given by:-

$$L_D = \left(\frac{\varepsilon_r \varepsilon_o k}{Tq^2 C_b} \right)^{\frac{1}{2}} \qquad (8)$$

Here ε_o and ε_r are the permittivities of free-space and the sample, respectively, C_b is the concentration of the bulk majority carrier with charge q. For a solid with $\varepsilon \sim 10$ and $C_b \sim 10^{22}$ m^{-3} and $T\sim$ 600 K, this leads to a Debye length of ~ 50 nm and a space charge width of approximately two times that value. Thus the effective boundary width contributing to enhanced conductivity may be many times greater than the boundary core width. The qualitative effect on ζ_o as the grain size decreases is shown schematically in Fig. 14. Clearly, this increased defect concentration will translate into enhanced diffusion.

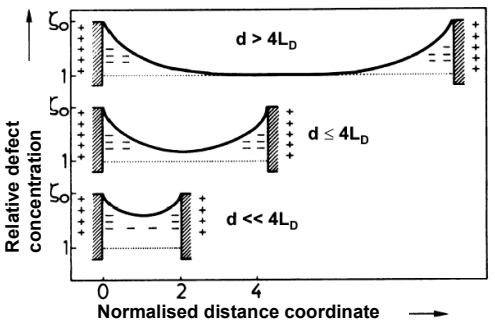

Fig. 14. Defect profiles in structures with dimension, d. The bulk defect concentration is not reached when $d<<4L$, where L_D is the Debye length (after [85]).

The focus here will be on the effect of particle size on conductivity rather than dispersed ionic conductors, for which details can be found in [19]. Although there have been a number of studies in many cases the results are far from conclusive. A straightforward result was obtained for the study of the conductivity of nanocrystalline CaF_2 prepared by IGC and with a particle size of 9 nm [89,90]. As seen in Fig. 15 the conductivity is enhanced and data fit well to a space charge enhancement model. Analogous experimental results were also obtained by NMR studies on CaF_2 prepared by IGC [62,91] as well as on BaF_2 prepared by ball milling [92]. Similarly the very elegant study of alternating nanocrystalline films of CaF_2 and BaF_2 produced by molecular beam epitaxy provided good proof of the space charge model, as shown in Fig. 16; the conductivity increased as the thickness of the layers decreased [93]. Less clear-cut are results for $LiNbO_3$ [94-98]. The results for ball-milled samples with a grain size of 23 nm showed a very enhanced motion for Li ions from the ^{7}Li NMR signal and conductivities were comparable, although somewhat lower than in the amorphous material [96,97]. However, EXAFS studies of ball-milled $LiNbO_3$ indicated that it contained some 50% amorphous material and that conductivity and NMR measurements for similar sized sol-gel samples were similar, although slightly higher, than bulk material [98].

A number of oxides exhibit fast oxygen ion conductivity and have applications as membranes in solid oxide fuel cells (SOFC) [99] and oxygen permeation membranes [100].

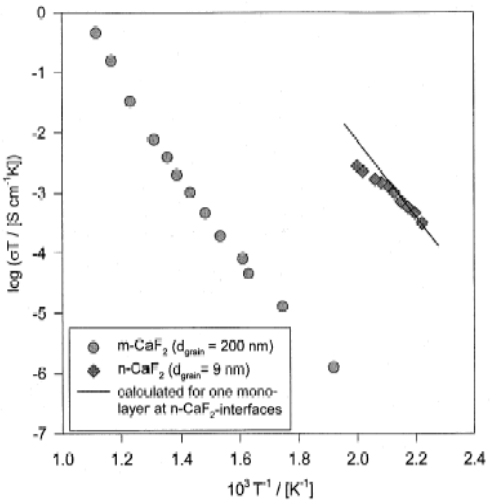

Fig. 15. Temperature dependence of the conductivities of nano- and micro-crystalline CaF_2 derived from the high-frequency semicircles. The line represents the estimated conductivities assuming a pronounced space charge effect [85] (from [90]).

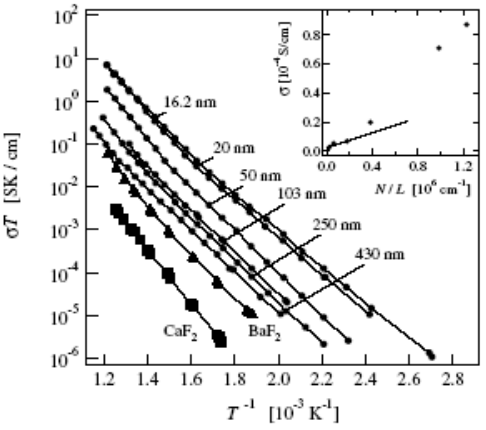

Fig. 16. Conductivity of CaF_2–BaF_2 layered heterostructures parallel to the films for different layer thicknesses, *L*. The inset shows the conductivity of the heterostructures at 320°C rising with the number of interfaces per unit length *N/L* (from [20] after [93]).

Thus it is not surprising that there has been interest in nanocrystalline samples where there is potential for increased conductivity and the potential for lower temperature operation of the membrane. Thus there have been a number of studies of nanocrystalline zirconia as a common SOFC membrane is cubic stabilized ZrO_2. Pure, bulk ZrO_2 adopts a monoclinic structure at normal temperatures, transforming at high temperature to a tetragonal and then cubic phase. The addition of aliovalent dopants, such as yttrium (YSZ) or calcium (CSZ) at low concentrations stabilize the tetragonal phase and at higher concentrations (>8% for yttrium) the cubic phase. Large cubic stabilized crystals can be grown for diffusion studies. In addition to stabilizing the cubic phase the dopants are compensated by oxygen ion vacancies and the conductivity is increased. Sol-gel prepared pure ZrO_2 can be cubic or tetragonal dependent on the grain size, usually tetragonal for grains >5 nm. ^{18}O tracer diffusion studies have been made on nanocrystalline samples prepared by magnetron sputtering of the metals and subsequent oxidation followed by compaction [101-103]. The particle sizes were 80-100 nm and the pure ZrO_2 was in the monoclinic phase. The experiments on pure ZrO_2 showed an interface diffusion coefficient some 3-4 orders of magnitude greater than in the crystallites, the latter having a slightly higher activation energy. The data for pure nanocrystalline material are shown in Fig. 17. The diffusion coefficients are lower than for CSZ and YSZ crystals, however it must be remembered that the latter materials are heavily doped. The ^{18}O diffusion in nanocrystalline ZrO_2 doped with 6.9% Y_2O_3 also showed an interfacial contribution that was more than three orders of magnitude greater than within the grains.

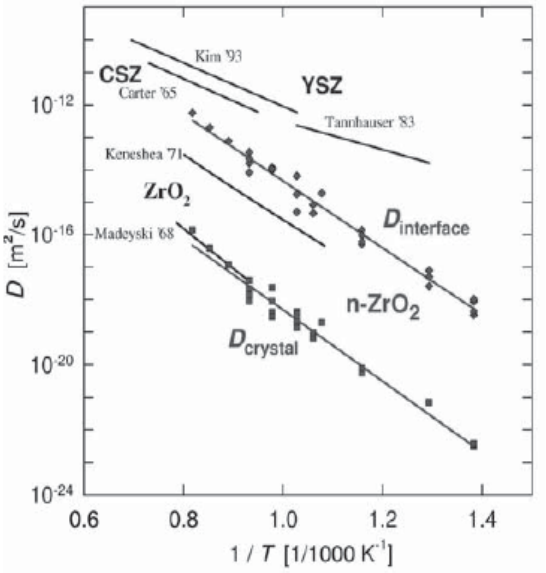

Fig. 17. Oxygen diffusion at interfaces and in the crystals of undoped, nanocrystalline ZrO_2. Bulk diffusion in CSZ and YSZ are also shown. (after [101]).

The available conductivity data for nanocrystalline ZrO_2 is perplexing. Firstly, conductivity studies of bulk ZrO_2 show that the grain boundary conductivity is 2 to 3 orders of magnitude *less* than the bulk conductivity [104-108]. This has been attributed to the segregation of impurities, notably silicon, into the grain boundaries to form blocking siliceous phases. The fact that decreasing the grain size led to a rapid increase in the grain boundary conductivity at sizes below 1000 nm provides some support for this model [109]; as the total grain boundary volume increases there is insufficient impurity to block the grains. However, it is worth noting that a contribution to grain boundary

blocking has also been proposed due to oxygen vacancy depletion in the grain boundary space charge layer [110]. Nanocrystalline ZrO_2 doped 2-3% Y_2O_3 with a grain size of 35 and 50 nm was prepared by IGC and the bulk and grain boundary conductivities were similar to those for normal ceramic samples [111]. A similar lack of conductivity enhancement was found in nanocrystalline YSZ with a grain size of 90 nm [112]. An exception to these results was the studies of nanocrystalline films on sapphire substrates prepared by a polymer precursor route [113]. In this case there was a clear size dependence of the conductivity and at a grain size of 15 nm the conductivity enhancement over bulk material was about two orders of magnitude. It has been pointed out [114] that these unusual results may be due to an interaction with the substrate or the effects of humidity. However, a high conductivity has recently been observed in nanocrystalline YSZ films prepared by laser ablation on a MgO substrate [115] and was ascribed to an interfacial effect. Clearly the diffusion and conductivity data are incompatible, hence more work is required to resolve this problem.

Ceria, CeO_2, also has the cubic fluorite structure and is an excellent oxygen ion conductor when doped with a rare earth cation, usually Gd^{3+}. The conductivity of highly dense pure CeO_2 with a grain size of 10 nm showed an increase when compared to large grain samples [44]. However, the conductivity of the nanocrystalline sample showed a very strong dependence on oxygen partial pressure, indicating electronic conductivity. The increase in the electronic contribution was a factor of $\sim 10^4$ at atmospheric pressure suggesting a change in stoichiometry and loss of oxygen to form CeO_{2-x}. Similar large enhancements of the electronic conductivity were observed in nanocrystalline rare-earth doped ceria [116]. Detailed studies of the effect of the grain size on the complex conductivity behaviour of both pure and doped CeO_2 have led to a successful modelling of the results in terms of a space-charge model [117-119]. Titania, TiO_2, is also a mixed ionic-electronic conductor and studies of 35 nm nanocrystalline anatase phase material indicated an increase in the ionic conductivity [120-122]. However, there is debate about the nature of the point defects in TiO_2 and the nature of the major charge carrier, hence the observed enhancement awaits explanation.

4. Conclusions

This contribution was aimed at providing an overview of the field rather than a comprehensive accumulation of the available data. The focus has been on the experimental work and it has not been possible to include work on computer simulations, which is making important contributions to the modelling of grain boundary structures [123] and plastic deformation [124]. Similarly the more complex situation of nanocrystalline composites has not been covered here. At this stage of the development of the field some conclusions can be deduced:-

- The method of sample preparation plays a key role in determining the atomic transport.
- In well-compacted nanocrystalline metal samples the commonly observed enhanced diffusion can be assigned to diffusion along grain boundaries.
- There is reliable evidence for enhanced diffusion in simple ionic solids that can be attributed to space-charge layer effects at the interfaces between grains.

- The evidence for enhanced diffusion in nanocrystalline oxides is clear from tracer diffusion experiments, however the conductivity data for these systems is still controversial. Some of these materials are mixed conductors and changing the grain size changes the conduction mechanism.

There is clearly scope for more experimental work in this area and important problems to resolve. The role of sample preparation has now been resolved for many systems and this should help in avoiding some of the complications found in early work. For the particular case of ionic materials there appears to be a need for more studies of diffusion rather than conductivity. In this respect, a greater role could be played by NMR methods with the use of ^{18}O offering possibilities to shed more light on the problems found in nanocrystalline oxides.

Acknowledgements

I wish to thank Dr. Shelley Savin for her contribution to the work on nanocrystals at Kent and the EPSRC for grant GR/S61881/01 that supports our work in this area.

References

[1] M.C. Roco, JOM-J. Minerals Metals and Materials Soc., 54 (2002) 22.
[2] H. Gleiter, Prog. Mater. Sci., 33 (1989) 223.
[3] H. Gleiter, Adv. Mater., 1992, 4, (1992) 474.
[4] A. Henglein, Chem. Rev., 89, (1989) 1061.
[5] H. Weller, Angew. Chem., Int. Ed. Engl., 32 (1993) 41.
[6] R.W. Siegel, G.E. Fougere, Nanostructured Mater., 6 (1995) 205.
[7] H. Gleiter, Acta mater., 48 (2000) 1.
[8] P. Moriarty, Rep. Prog. Phys., 64 (2001) 297.
[9] R.Würschum, U. Brossmann, H-E. Schaefer, in Nanostructured Materials—Processing, Properties, and Applications, ed C C Koch (Norwich: Noyes Publications) (2002) p. 267.
[10] A.S. Edelstein, R.C. Cammarata, ed. Nanomaterials: Synthesis, Properties and Applications (Institute of Physics, Bristol, UK) (2002).
[11] J.V. Stark, D.G. Park, I. Lagadic, K.J. Klabunde, Chem. Mat., 8 (1996) 1904.
[12] J.V. Stark, K.J. Klabunde, Chem. Mat., 8 (1996) 1913.
[13] Y. Sun, Y. Xia, Science, 298 (2002) 2176.
[14] O,B. Koper, K.J. Klabunde, Chem. Mat., 9 (1997) 2481.
[15] R. W. Siegel, Annu. Rev. Mater. Sci. 21 (1991) 559.
[16] S.C. Tjong, H. Chen, Materials Science and Engineering R, 45 (2004) 1.
[17] S. Takeuchi, Scr. Mater., 44 (2001) 1483
[18] L. Lu, M.L. Sui, K. Lu, Science, 287 (2000) 1463.
[19] R. Würschum, Rev. Metall. 96 (1999) 1547.
[20] P. Heitjans, S. Indris, J. Phys.: Condens. Matter, 15 (2003) R1257.

[21] H. Gleiter, in Deformation of Polycrystals: Mechanisms and Microstructures, eds N. Hansen, A. Horsewell, T. Lefferes, H. Lilholt (Riso National laboratory, Roskilde, Denmark) (1981) p. 15.
[22] J. Ying, J. Aerosol. Sci., 24 (1993) 315.
[23] D.H. Pearson, A.S. Edelstein, Nanostruct. Mater., 11 (1999) 1111.
[24] G. Gonzalez, J.A. Freites, C.E. Rojas, Scr. Mater., 44 (2001) 1883.
[25] P. Taneja, R. Chandra, R. Banerjee, P. Ayyub, Scr. Mater., 44 (2001) 1915.
[26] G.L. Messing, S.C. Zhang, G.V. Jayanthi, J. Am. Ceram. Soc., 76 (1993) 2707.
[27] C.J. Brinker, J.W. Scherer, Sol–Gel Science: The Physics and Chemistry of Sol–Gel Processing, (Academic Press, Boston) (1990).
[28] A.C. Pierre, Introduction to Sol–Gel Processing, (Kluwer Academic Publishers, Boston) (1998).
[29] A.V. Chadwick, G. Mountjoy, V.M. Nield, I.J.F. Poplett, M.E. Smith, J.H. Strange, M.G. Tucker, Chem. Mater., 13 (2001) 1219.
[30] S.R. Davis, A.V. Chadwick, J.D. Wright, J. Phys. Chem. B, 101 (1997) 9901.
[31] H.J. Fecht, Nanostruct. Mater., 6 (1995) 33.
[32] C.C. Koch, Nanostruct. Mater., 9 (1997) 13.
[33] L.M. Cukrov, T. Tsuzuki, P.G. McCormick, Scr. Mater., 44 (2001) 1787.
[34] S. Indris, D. Bork, P. Heitjans, J. Mater. Synth. Process. 8 (2000) 245.
[35] J. Ding, T. Tsuzuki, P.G. McCormick, R. Street, J. Phys. D, 29 (1996) 2365.
[36] E. Baburaj, K. Hubert, F. Froes, J. Alloys Compd., 257 (1997) 146.
[37] Scholz, G., Stosser, R., Klein, J., Silly, G., Buzaré, J.Y., Laligant, Y. and Ziemer, B., J. Phys.: Condens. Matter, 14 (2002) 14, 2101.
[38] A. Weibel, R. Bouchet, F. Boule'h. P. Knauth, Chem. Mat., (2005) in press.
[39] H.P. Klug and L.E. Alexander, X-ray diffraction procedures for polycrystalline and amorphous materials, (Wiley Interscience Publication, New York) (1974).
[40] D. Balzar, Defect and Microstructure Analysis from Diffraction, (Oxford University Press, New York) (1999).
[41] J. Rouquerol, F. Rouquerol, K.S.W. Sing, Adsorption by powders and porous solids, (Academic Press, London) (1999).
[42] T. Allen, Particle Size Measurement; Volume I, (Kluwer Academic Press, Netherlands) (1999).
[43] G.T. Thomas, R.W. Siegel, J.A. Eastman, Scr. Metall., 24 (1990) 201.
[44] Y.-M. Chiang, E.B. Lavik, I. Kosacki, H.L. Tuller, J.Y. Ying, J. Electroceramics, 1 (1997) 7.
[45] Th.E. Weirich, M. Winterer, S. Seifried, H. Hahn, F. Fuess, Ultramicroscopy, 81 (2000) 263.
[46] R. Würschum, G. Soyez, H-E. Schaefer, Nanostruct. Mater., 3 (1993) 225.
[47] T. Haubold, R. Birringer, B. Lengeler, H. Gleiter, Phys. Lett. A, 135 (1989) 461.
[48] S. de Panfilis, F. d'Acapito, V. Haas, H. Konrad, J. Weissmüller, F. Boscherini, Phys. Lett. A, 207, (1995) 397.
[49] A.V. Chadwick, G.E. Rush, Characterisation of nanocrystalline metal oxides by XAS, in Nanocrystalline Materials, eds. P. Knauth and J. Schoonman, (Kluwer, New York) (2002) chapter 5.

[50] B.K. Teo, D.C. Joy, eds., EXAFS Spectroscopy; Techniques and Applications, (Plenum Press, New York) (1980).
[51] T.M. Hayes, J.B. Boyce, Solid State Phys., 37 (1982) 173.
[52] D.C. Koningsberger, R. Prins, eds. X-Ray Absorption, (Wiley, New York) (1988).
[53] Y.R. Wang, K.Q. Lu, D.H. Wang, Z.H., Wu, Z.Z. Fang, J. Phys.; Condens. Matter, 6 (1994) 633.
[54] Z. Qi, C., Shi, Y. Wei, Z. Wang, T. Liu, T. Hu, Z. Zhan, F. Li, J. Phys.; Condens. Matter, 13 (2001) 11503.
[55] G.E. Rush, A.V. Chadwick, I. Kosacki, H.U. Anderson, J. Phys. Chem. B, 104 (2000) 9597.
[55] A.V. Chadwick, M.J. Pooley, K.E. Rammutla, S.L.P. Savin, A. Rougier, J. Phys.: Condens. Matter, 15 (2003) 431.
[56] A.V. Chadwick, M.J. Pooley, S.L.P. Savin, Physica status solidi (c), 2 (2005) 302.
[58] E.A. Stern, R.W. Siegel, M. Newville, P.G. Sanders, D. Haskel, D., Phys. Rev. Lett., 75 (1995) 3874.
[59] P. Heitjans, Solid State Ionics, 18/19 (1989) 50.
[60] H. Mehrer, Diffusion in Condensed Matter - Methods, Materials, Models, eds P. Heitjans, J. Kärger (Springer, Berlin) (2005) chapter 1.
[61] J. Crank, The Mathematics of Diffusion, (Clarendon Press, Oxford) (1995).
[62] P. Heitjans, A. Schirmer, S. Indris, Diffusion in Condensed Matter - Methods, Materials, Models, eds P. Heitjans, J. Kärger (Springer, Berlin) (2005) chapter 9.
[63] A.V. Chadwick, J.C.S. Faraday I, 86 (1990) 1157.
[64] A.B. Lidiard, Handbuch der Physik, XX (1957) 246.
[65] F. Bénière, in Physics of Electrolytes ed J Hladik, (Academic Press, London) (1972) p. 203.
[66] A.V. Chadwick, Phil. Mag., A64 (1991) 983.
[67] J.R. McDonald, ed., Impedance Spectroscopy, (Wiley, New York) (1983)
[68] S.P.S. Badwal, S. Rajendran, Solid State Ionics, 70/71 (1994) 83.
[69] J. Fleig, Solid State Ionics, 131 (2000) 117.
[70] J.E. Bauerle, J. Phys. Chem., 30 (1969) 2657.
[71] J. Philibert, Atom movement, diffusion and mass transport in solids, (Les Éditions de Physique, Paris) (1991).
[72] A. Atkinson, C. Monty, in, Surfaces and Interfaces of Ceramic Materials, eds : L.C. Dufour et al. (Kluwer Academic, Dordrecht) (1989) p. 273.
[73] R. Würschum, S. Herth, U. Brossmann, Adv. Eng. Mat., 5 (2003) 365.
[74] J. Horváth, R, Birringer, H.Gleiter, Solid State Commun., 62 (1987) 319.
[75] T. Mütschele, R. Kirchheim, Scripta Mater., 21 (1987) 135.
[76] H. Tamimoto, P. Farber, R Würschum, R.Z. Valiev, H.-E. Schaefer, Nanostructured Mater., 12 (1999) 681.
[77] M. Lubbehusen, H. Mehrer, Acta Metall. Mater., 3 (1990) 283.
[78] J. Benardini, P. Gas, E.D. Hondros, M.P. Seah, Proc. Roy. Soc. London, A379 (1982) 159.
[79] R. Würschum, P. Farber, R. Dittmar, P. Scharwaechter, W. Frank, H.-E. Schaefer, Phys. Rev. Lett., 79 (1997) 4918.

[80] S.V. Divinski, F. Hisker, Y.-S. Kang, J.-S. Lee, Chr. Herzig, Acta Mater., 52 (2004) 645.
[81] S.V. Divinski, F. Hisker, Y.-S, Kang, J-S. Lee, Chr. Herzig, Z. Metallkd., 93 (2002) 265.
[82] S.V. Divinski, F. Hisker, Y.-S, Kang, J-S. Lee, Chr. Herzig, Interface Sci., 11 (2002) 67.
[83] Z.B. Wang, N.R. Tao, W.P. Tong, J. Lu, K. Lu, Acta Mater., 51 (2003) 4319.
[84] C.C. Liang, J. Electrochem. Soc., 120 (1973) 1289.
[85] J. Maier, Solid State Ionics, 23 (1987) 59.
[86] J. Maier, J. Electrochem. Soc., 134 (1987) 1524.
[87] J. Maier, Prog. Solid State Chem., 23 (1995) 171.
[88] J. Maier, Solid State Ionics, 131 (2000) 13.
[89] W. Puin, P. Heitjans, Nanostructured Materials, 6 (1995) 885.
[90] W. Puin, S. Rodewald, R. Ramlau, P. Heitjans, J. Maier, 2000 Solid State Ionics, 131 (2000) 159.
[91] W. Puin, P. Heitjans, W. Dickenscheid, H. Gleiter, Defects in Insulating Materials, eds O. Kanert, J.-M. Spaeth (World Scientific, Singapore) (1993) p. 137
[92] P. Heitjans, S. Indris, J. Mater. Sci., 39 (2004) 5091.
[93] N. Sata, K. Ebermann, K. Eberl, J. Maier, Nature, 408 (2000) 946.
[94] D. Bork, P. Heitjans, J. Phys. Chem. B, 105 (2001) 9162.
[95] D. Bork, P. Heitjans, J. Phys. Chem. B, 102 (1998) 7303.
[96] M. Wilkening, D. Bork, S. Indris, P. Heitjans, Phys. Chem. Chem. Phys., 4 (2002) 3246.
[97] M. Masoud, P. Heitjans, Defect and Diffusion Forum, 237-240 (2005) 1016.
[98] A.V. Chadwick, M.J. Pooley, S.L.P. Savin, Physica status solidi (c), 2 (2005) 302.
[99] B.C.H. Steele, Phil. Trans. Roy. Soc., A., 354 (1996) 1695.
[100] W.C. Maskell, Solid State Ionics, 134 (2000) 43.
[101] U. Brossman, R. Würschum, U. Södervall, J. App. Phys., 85 (1999) 7636.
[102] G. Knöner, K. Reimann, R. Röwer, H.-E. Schaefer, Proc. Nat. Acad. Sci., 100 (2003) 2870.
[103] U. Brossman, G. Knöner, H.-E. Schaefer, R. Würschum, Rev. Adv. Mater. Sci., 6 (2004) 7.
[104] N.M. Beekmans, L. Heyne, Electrochim. Acta, 21 (1976) 303.
[105] T. van Dijk, A.J. Burggraaf, Phys. Status Solidi A, 63 (1981) 229.
[106] C.A. Leach, P. Tanev, B.C.H. Steele, J. Mater. Sci. Lett., 5 (1986) 893.
[107] S.P.S. Badwal, J. Drennan, J. Mater. Sci., 22 (1987) 3231.
[108] S.P.S. Badwal, A.E. Hughes, J. Eur. Ceram. Soc., 10 (1992) 115.
[109] M. Aoki, Y.-M. Chiang, I. Kosacki, J.R. Lee, H.L. Tuller, Y.-P. Liu, J. Am. Ceram. Soc., 79 (1996) 1169.
[110] X. Guo, W. Sigle, J. Fleig, J. Maier, Solid State Ionics, 154– 155 (2002) 555.
[111] P. Mondal, H. Hahn, Ber. Bunsenges Phys. Chem., 101 (1997) 1765.
[112] S. Jiang, J. Mat. Res., 12 (1997) 2374.
[113] I. Kosacki, B. Gorman, H.U. Anderson, in: T.A. Ramanarayanan, W.L. Worrell, H.L. Tuller, A.C. Kandkar, M. Mogensen,W. Gopel (Eds.), Ionic and Mixed Conductors, Vol. III, (Electrochemical Society, Pennington, NJ) (1998) p. 631.

[114] H.L. Tuller, Solid State Ionics, 131 (2000) 143.
[115] I. Kosacki, T. C.M. Rouleaub, P.F. Bechera, J. Bentley, D.H. Lowndes, Solid State Ionics, (2004) in press.
[116] Y.M. Chiang, E.B. Lavik, D.A. Blom, Nanostructured Mater., 9 (1997) 633
[117] A. Tschöpe, S. Kilassonia, B. Zapp, R. Birringer, Solid State Ionics, 149 (2002) 261.
[118] A. Tschöpe, Solid State Ionics, 139 (2001) 267.
[119] A. Tschöpe, S. Kilassonia, R. Birringer, Solid State Ionics, 173 (2004) 57.
[120] P. Knauth, H.L. Tuller, J. Appl. Phys., 85 (1999) 897.
[121] P. Knauth, J. Solid State Electrochem., 147 (2002) 115.
[122] P. Knauth, H.L. Tuller, Solid State Ionics, 136–137 (2000) 1215.
[123] H. Van Swygenhoven, D. Farkas, A. Caro, Phys. Rev. B, 62 (2000) 831.
[124] D. Wolf, V. Yamakov, S.R. Phillpot, A. Mukherjee, H. Gleiter, Acta Mater., 53 (2005) 1.